

Antiferroelectric Altermagnets: Antiferroelectricity Alters Magnets

Xunkai Duan^{1,2}, Jiayong Zhang^{1,3,4}, Ziye Zhu^{1,4}, Yuntian Liu^{1,5}, Zhenyu Zhang⁴, Igor Žutić^{1,5}, and Tong Zhou^{1,*}

¹*Eastern Institute for Advanced Study, Eastern Institute of Technology, Ningbo, Zhejiang 315200, China*

²*School of Physics and Astronomy, Shanghai Jiao Tong University, Shanghai 200240, China*

³*School of Physical Science and Technology, Suzhou University of Science and Technology, Suzhou 215009, China*

⁴*International Center for Quantum Design of Functional Materials (ICQD), and Hefei National Laboratory,*

University of Science and Technology of China, Hefei 230026, China

⁵*Department of Physics, University at Buffalo, State University of New York, Buffalo, New York 14260, USA*

(Received 7 September 2024; revised 6 January 2025; accepted 4 February 2025; published 13 March 2025)

Magnetoelectric coupling is crucial for uncovering fundamental phenomena and advancing technologies in high-density data storage and energy-efficient devices. The emergence of altermagnets, which unify the advantages of ferromagnets and antiferromagnets, offers unprecedented opportunities for magnetoelectric coupling. However, electrically tuning altermagnets remains an outstanding challenge. Here, we demonstrate how this challenge can be overcome by using antiferroelectricity and ferroelectricity to modulate the spin splitting in altermagnets, employing a universal, symmetry-based design principle supported by an effective model. We introduce an unexplored class of multiferroics: antiferroelectric altermagnets (AFEAM), where antiferroelectricity and altermagnetism coexist in a single material. From first-principles calculations, we validate the feasibility of AFEAM in well-established van der Waals metal thio(seleno)phosphates and perovskite oxides. We reveal the design of AFEAM ranging from two-dimensional monolayers to three-dimensional bulk structures. Remarkably, even a weak electric field can effectively toggle spin polarization in the AFEAM by switching between antiferroelectric and ferroelectric states. Our findings not only enrich the understanding of magnetoelectric coupling but also pave the way for electrically controlled spintronic and multiferroic devices.

DOI: 10.1103/PhysRevLett.134.106801

Rather than applying magnetic field, electric control is pursued to achieve faster and more energy-efficient manipulation of magnetism [1–3]. The nonvolatility of magnetic materials enables not only advances in high-density storage and neuromorphic computing [1–3], but also integrating electronics, spintronics, and photonics [4]. Multiferroics, with their magnetoelectric coupling and both (anti)ferroelectricity and magnetism, are excellent candidates for electrical control of magnetism and spin polarization [5–7]. This coupling could also elucidate fundamental phenomena, from probing dark matter to topological phase transitions [8,9].

Since common ferromagnets are metallic, while ferroelectric (FE) states are insulating, their coexistence in a single material is difficult [10]. Realizing multiferroics with typically insulating FE and antiferromagnets (AFM) is more feasible, while also supporting higher critical temperatures, no stray fields, and ultrafast dynamics, desirable for spintronics [11–14]. However, the absence of spin polarization in conventional AFM limits their utility in multiferroics.

Building on the understanding of AFM with the nonrelativistic spin splitting [15–20], the discovery of

altermagnets (AM) [21,22] with zero net magnetization and momentum-dependent spin splitting [23–29], could overcome these challenges. The resulting phenomena with AM already include generating spin-polarized currents [30], giant magnetoresistance [31–33], nontrivial superconductivity [34–36], anomalous Hall effect [37–40], and other interesting spintronic behavior [41–44]. Despite that AM unify many advantages of AFM and ferromagnets (FM), which could be important for magnetoelectric coupling, integrating ferroelectricity to control AM in multiferroic systems is largely missing.

In this work, we reveal how many challenges to control AM can be overcome using (anti)ferroelectricity and a universal design principle illustrated in Fig. 1. We introduce an unexplored class of multiferroics: antiferroelectric altermagnets (AFEAM) which support electric control of spin in a single material using a small electric field and demonstrate exciting magnetoelectric coupling. Their opposite spin lattices are connected through rotation symmetry R , which can also include a combination of translation or inversion, induced by the AFE environment to yield AM with spin polarization, $P_S \neq 0$. An applied electric field, ϵ , transforms AFEAM into conventional ferroelectric AFM (FEAFM) with $P_S = 0$, due to the direct translation, t , of the spin lattices in the FE environment. This transition enables electric control of P_S . The mechanism and

*Contact author: tzhou@eitech.edu.cn

universality of our design principle are further demonstrated using an effective tight-binding (TB) model. To illustrate the practicality of our approach, we employ first-principles calculations to identify AFEAM in well-explored multiferroic materials, including (i) two-dimensional (2D) van der Waals (vdW) metal thio(seleno)phosphates [45] such as CuMoP₂S(Se)₆ and CuWP₂S(Se)₆, where AFEAM persists from monolayers (MLs) to bulk, independent of layer thickness and (ii) 3D multiferroic transition-metal-oxide perovskites [46], such as BiCrO₃.

Our design principle for the AFEAM and the electric control of P_S can be understood from the role of the AFE (FE) environment on AFM shown in Fig. 1, which leads to the AM (conventional AFM). The influence of (anti) ferroelectricity on magnetism is analyzed using the exchange operation approach [47,48] and spin group theory [49–53], employed to study momentum-dependent spin splitting in AM. The spin-dependent bands are described by the Kohn-Sham equations

$$\left[\frac{1}{2}(\mathbf{k} - i\nabla)^2 + V_\alpha \right] \psi_\alpha(\mathbf{k}) = E_\alpha(\mathbf{k}) \psi_\alpha(\mathbf{k}), \quad (1)$$

where \mathbf{k} is the wave vector, V_α is the Kohn-Sham potential with α for spin-up (\uparrow) and spin-down (\downarrow). $E(\mathbf{k})$ and $\psi(\mathbf{k})$ denote the eigenvalue and wave function. Exchange operations O are the symmetry operations in the geometric space group that exclude spin configurations. They map the spin-up to the spin-down lattices as $OV\uparrow O^{-1} = V\downarrow$. The spin degeneracy and splitting are determined for $Ok = \mathbf{k}$, $E\uparrow(\mathbf{k}) = E\downarrow(\mathbf{k})$, and for $Ok \neq \mathbf{k} = \mathbf{k}'$, $E\uparrow(\mathbf{k}) \neq E\downarrow(\mathbf{k}) = E\downarrow(\mathbf{k}')$ [47,48].

For FEAFM, with net electric polarization, $\mathbf{P} \neq 0$, spin lattices are related by direct t . Since $t\mathbf{k} = \mathbf{k}$ for all \mathbf{k} , the bands are spin-degenerate in the whole Brillouin zone, giving the conventional AFM with $P_S = 0$ as in Fig. 1(b). In contrast, for AFEAM, with alternating electric polarization ($\mathbf{P} = 0$), its spin lattices cannot be connected by a direct t , but by R (commonly C_2t), leading to $P_S = 0$ only along specific paths where $R\mathbf{k} = \mathbf{k}$, while $P_S \neq 0$ elsewhere, defining AM as in Fig. 1(a).

Considering AFE and FE configurations are locked with AM and AFM states and their transition can be flexibly reversed through ϵ [46,54], we propose ϵ -controlled AFEAM and FEAFM transitions to toggle the P_S as shown in Fig. 1. This electric control of P_S relying on straightforward conditions, where the symmetry of AFM can be switched between $[C_2\|t]$ and $[C_2\|R]$, offers a novel and accessible mechanism for realizing magnetoelectric coupling.

To illustrate our design principle, we develop a TB model based on a general 2D rectangular lattice with nested AFM order (Fig. 2). This setup includes the essential elements of our proposal: AFM sublattices with AFE (FE) configurations connected by R (t) symmetry. The minimal model, to capture the influence of AFE and FE

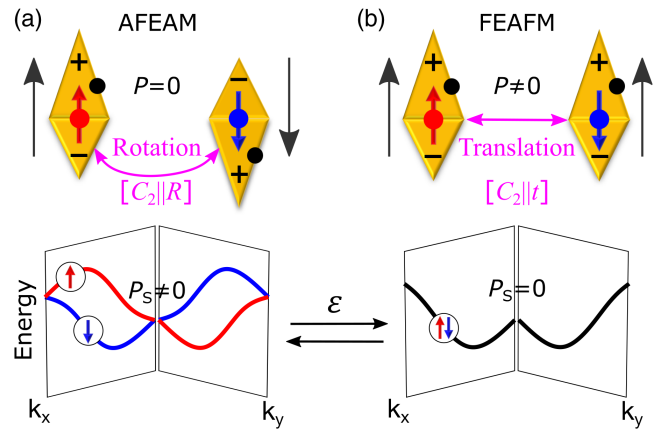


FIG. 1. The design principle for AFEAM and FEAFM. Magnetic atoms with opposite spins (red and blue arrows) constructing AFM sublattices. Antiparallel (parallel) local electric polarizations (black arrows), from the asymmetric charge distributions around these atoms due to displaced nonmagnetic atoms (black dots), show AFE (FE) states without (with) net electric polarization, \mathbf{P} . (a) AFEAM: magnetic sublattices are connected by rotation, R , resulting in AM with spin polarization, $P_S \neq 0$. (b) FEAFM: magnetic sublattices are directly connected by translation, t , leading to a conventional AFM with $P_S = 0$. The AFEAM and FEAFM can be switched by an electric field, ϵ , enabling an electric control of P_S .

configurations on AM, incorporates up to the third-nearest-neighbor hopping

$$H = \left(\sum_{i,j} (f_i^{\eta_j} c_i^\dagger c_{i+\eta_j} + g_i^{\kappa_j} c_i^\dagger c_{i+\kappa_j} + h_i^{\delta_j} c_i^\dagger c_{i+\delta_j}) + \text{H.c.} \right) + M_{A,B} \sum_{i \in A,B} c_i^\dagger \sigma_z c_i. \quad (2)$$

Here, c_i^\dagger (c_i) are electron creation (annihilation) operators at site i and σ is the Pauli matrix. The first three terms describe hoppings between first (NN), second (2NN), and third (3NN) nearest-neighbors with hopping parameters $f_i^{\eta_j}$, $g_i^{\kappa_j}$, and $h_i^{\delta_j}$, where η_j , κ_j , and δ_j are the vectors connecting site i to its NN, 2NN, and 3NN sites. The last term indicates AFM exchange fields on sublattices A and B with $M_A = -M_B$.

The emergence of AM arises from the inequivalence between magnetic sublattices [21]. While the NN and 2NN hoppings do not contribute to AM as they are sublattice equivalent under both AFE and FE configurations, as discussed in Supplemental Material [55], 3NN hoppings are dependent on sublattices and (A)FE configurations, playing a crucial role in altermagnetism. In FEAFM, $[C_2\|t]$ symmetry ensures that 3NN hoppings are also equivalent between opposite sublattices ($h_A^{\delta_{1-6}} = h_B^{\delta_{1-6}}$) [Fig. 2(b)]. Consequently, the calculated bands exhibit spin degeneracy, characteristic of conventional AFM [Fig. 2(d)].

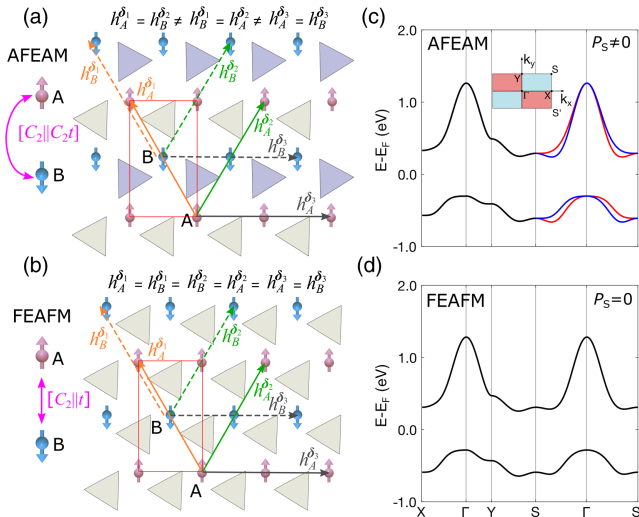


FIG. 2. Schematic of 2D rectangular magnetic sublattices *A* and *B* with AFE (distinct triangles) and FE (identical triangles) configurations, forming (a) AFEAM with $[C_2||C_2t]$ symmetry and (b) FEAFM with $[C_2||t]$ symmetry, respectively. The solid (dashed) arrows indicate 3NN hopping vectors (δ_{1-3}) in *A* (*B*) sublattice with hopping strengths $h_A^{\delta_{1-3}} = h_B^{\delta_{1-3}}$. The other three hopping vectors ($\delta_{4-6} = -\delta_{1-3}$) are not shown as the hopping strengths along opposite directions are identical ($h_{A,B}^{\delta_{4-6}} = h_{A,B}^{\delta_{1-3}}$). (c) Calculated bands for (a) AFEAM using TB model with parameters $f_{A,B}^{\eta_{1-6}} = 0.10$ eV, $g_{A,B}^{\kappa_{1-6}} = 0.06$ eV, $h_A^{\delta_{1,4}} = h_B^{\delta_{2,5}} = 0.04$ eV, $h_A^{\delta_{2,5}} = h_B^{\delta_{1,4}} = 0.01$ eV, $h_A^{\delta_{3,6}} = h_B^{\delta_{3,6}} = 0.03$ eV, and $M_A = -M_B = 0.45$ eV. The black, red, and blue denote the spin-degenerate, -up, and -down bands, respectively. The inset diagram indicates the P_S sign in the Brillouin zone of (a). (d) Same as (c), but for (b) FEAFM with $h_A^{\delta_{1-6}} = h_B^{\delta_{1-6}} = 0.03$ eV.

In contrast, in AFEAM, the AFE configuration breaks *t* symmetry, leaving magnetic sublattices connected by $[C_2||C_2t]$. This symmetry breaking alters the 3NN hopping strengths such that hopping along $\delta_{1,4}$ in sublattice *A* ($h_A^{\delta_{1,4}}$) differs from that in sublattice *B* ($h_B^{\delta_{1,4}}$) but equals the hopping along $\delta_{2,5}$ ($h_A^{\delta_{2,5}}$) in sublattice *B*, and vice versa, i.e., $h_A^{\delta_{1,4}} = h_B^{\delta_{2,5}} \neq h_B^{\delta_{1,4}} = h_A^{\delta_{2,5}} \neq h_A^{\delta_{3,6}} = h_B^{\delta_{3,6}}$ as depicted in Fig. 2(a). This directional alternation induces AM, as confirmed by the calculated bands in Fig. 2(c). This effective model, clearly demonstrating our AFEAM design, also provides a versatile framework for exploring AM mechanisms and applications.

Following the above TB model, we first examine our design principle for AFEAM and ϵ -controlled P_S in the family $\text{CuMP}_2\text{S}(\text{Se})_6$, where $M = \text{Cr, Mo, W}$, known for its 2D multiferroic properties [62–67]. The Cu ions have a zigzag vertical shift from the mid-plane of its structure, inducing a local out-of-plane electric polarization with AFE order, while the Cr/Mo/W atoms induce magnetism constructing spin lattices as in Fig. 3(a). Applying ϵ can align the Cu ions to the same side within the vertical layer,

producing a FE phase [Fig. 3(b)], as observed in recent experiments [64–66].

To reveal the magnetic order and electronic structure of $\text{CuMP}_2\text{S}(\text{Se})_6$, we first explore their MLs and then study thicker films and bulk material through vdW stacking. We consider three typical magnetic configurations: FM, stripe AFM (sAFM) in Fig. 3, and zigzag AFM in Supplemental Material [55]. Our calculations show that the ML $\text{CuCrP}_2\text{S}(\text{Se})_6$ favors FM, while MLs of $\text{CuMoP}_2\text{S}(\text{Se})_6$ and $\text{CuWP}_2\text{S}(\text{Se})_6$ favor sAFM as discussed in Supplemental Material [55], consistent with the previous studies and experiments [62–66]. This *M*-type dependency is attributed to the combined effect [63,68,69] of the crystal field splitting and the exchange interaction [55]. While previous studies have mainly focused on FM $\text{CuCrP}_2\text{S}(\text{Se})_6$, the AFM $\text{CuMoP}_2\text{S}(\text{Se})_6$ and $\text{CuWP}_2\text{S}(\text{Se})_6$ are largely overlooked as AFM are often deemed less interesting. However, these AFM are excellent candidates for our AFEAM design in Fig. 1.

Without losing generality, we consider ML CuWP_2S_6 (CWPS) to demonstrate our AFEAM design. Additional results for other $\text{CuMP}_2\text{S}(\text{Se})_6$ compounds are provided in Supplemental Material [55]. With ignoring the magnetism, the space group of AFE ML CWPS is $P2_1$ with symmetry $\{E, C_{2y}t\}$, for the identity and screw axis along *y*. Instead, considering the ground-state sAFM order, its space group is lowered to P_1 containing only $\{E\}$ with missing $C_{2y}t$ acting as the key exchange operations that define the electronic structures through the spin group $[C_2||C_{2y}t]$, as shown in Fig. 3(a).

The exchange operation of $C_{2y}t$ satisfies $C_{2y}t\mathbf{k}(\Gamma - Y) = \mathbf{k}(\Gamma - Y)$, where $\mathbf{k}(\Gamma - Y)$ indicates the \mathbf{k} points along the $\Gamma - Y$ path [Fig. 3(c)]. Moreover, considering inversion *I*, we can get an additional exchange operation, $IC_{2y}t$, which satisfies $IC_{2y}tV_\uparrow(IC_{2y}t)^{-1} = V_\downarrow$ and $IC_{2y}t\mathbf{k}(\Gamma - X) = \mathbf{k}(\Gamma - X)$. Thus, we obtain $E_\uparrow(X - \Gamma - Y) = E_\downarrow(X - \Gamma - Y)$, giving the spin degeneracy along $X - \Gamma - Y$. In contrast, for other paths lacking specific symmetry operations, such as $S - \Gamma - S'$, their bands are spin polarized. Furthermore, the relation $C_{2y}t\mathbf{k}(\Gamma - S) = \mathbf{k}(\Gamma - S')$ introduces $E_\uparrow(\Gamma - S) = E_\downarrow(\Gamma - S')$, resulting in opposite P_S along such two paths with a *d*-wave character [Fig. 3(c)]. The spin splitting in CWPS is up to 120 meV, which can be experimentally distinguished by the angle-resolved photo-emission spectroscopy [23,70]. Since, unlike the spin-orbit coupling (SOC), AM breaks the time-reversal symmetry and can display typical ferromagnetic properties, we can use spin transport to distinguish antiferromagnetic and SOC spin splitting, as discussed in Supplemental Material [55]. For FE-sAFM CWPS, there is a direct *t* operation as O [Fig. 3(b)] satisfying $t\mathbf{k} = \mathbf{k}$ for all \mathbf{k} , thus there is no spin splitting throughout the Brillouin zone, giving a conventional AFM [Fig. 3(d)]. This phenomenon, where AFE states produce AM, while FE states revert to conventional AFM, illustrates our design principle and confirms CWPS as AFEAM.

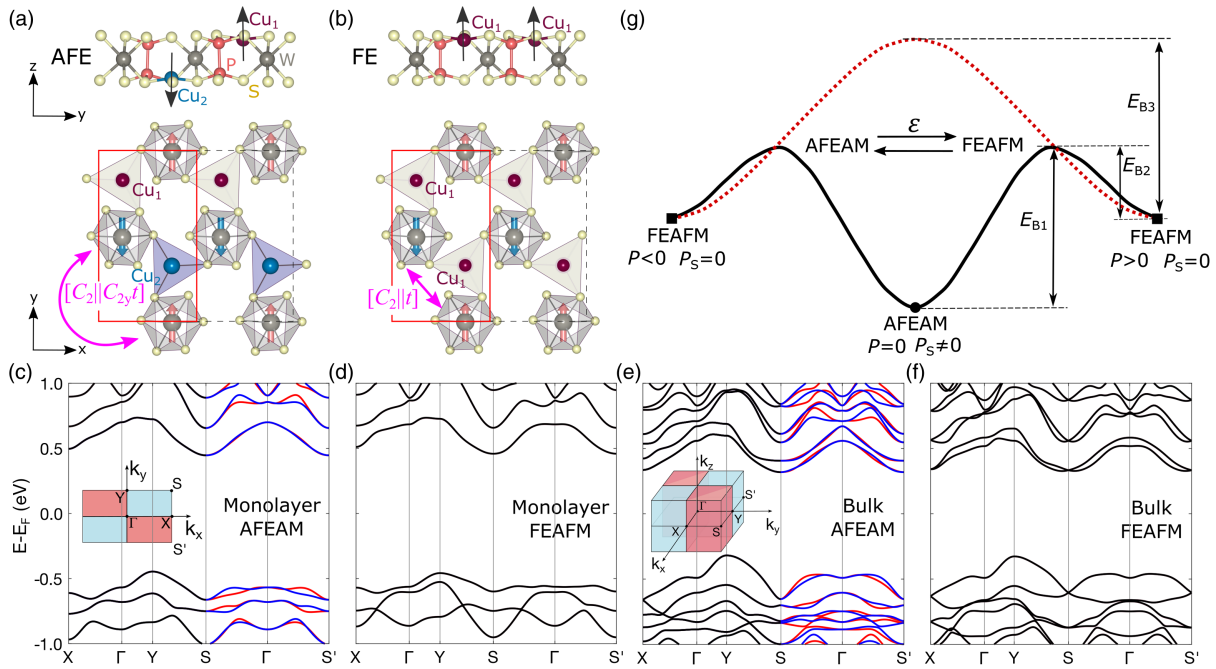


FIG. 3. (a) and (b) Structures and magnetic ground state (sAFM) of ML AFE and FE CuWP₂S₆, characterized by $[C_2||C_2t]$ and by $[C_2||t]$ symmetry, respectively. (c) and (d) Calculated bands for (a) and (b), where the black, red, and blue denote the spin-degenerate, -up, and -down bands, respectively. (e) and (f) Same as (c) and (d) but for bulk CuWP₂S₆. The insets in (c) and (e) show P_S sign in their Brillouin zones. (g) Calculated kinetic switching pathways between negative ($\mathbf{P} < 0$) and positive ($\mathbf{P} > 0$) FE states through AFE (solid line) or PE (dotted line) states in ML CuWP₂S₆. E_{B1} , E_{B2} , and E_{B3} indicate the energy barriers of AFE-to-FE, FE-to-AFE, and FE-to-PE-to-FE states, respectively. P_S can be electrically toggled by switching between AFEAM and FEAFM.

Considering CWPS is a vdW material, its properties of the bulk structure and few-layer films [55] are expected to resemble those of the MLs. This expectation is supported by our first-principles calculations, which confirm both the bulk and film forms of CWPS retain the same intralayer AFE-sAFM order and show AFEAM behavior, as in Fig. 3(e) and Supplemental Material [55]. We find the sign of the \mathbf{P}_S in the bulk CWPS does not vary with k_z , exhibiting altermagnetic spin splitting for all k_z planes (even for $k_z = 0$). This behavior, distinct from the reported bulk AM [23–29], reflects the vdW nature of CWPS. Furthermore, by altering the AFE to FE order, bulk CWPS also switches from AFEAM to FEAFM [Fig. 3(f)]. For CWPS films, our calculations confirm their electronic structures are consistent with those of their ML and bulk counterparts [55]. Such properties, independent of the layer thickness, facilitate the experimental realization of our proposal.

The AFE-to-FE transition typically occurs reversibly when the applied ϵ , with the energy E_ϵ , aligns the electric polarization by overcoming its energy barrier, E_{B1} , while the FE-to-AFE transition depends on the stability of the FE state [46,54]. An unstable FE state spontaneously reverts to the AFE ground state when the ϵ is removed [46], while a metastable FE state requires a reversed ϵ to overcome the metastability barrier, E_{B2} and return to the AFE state [54,71,72]. To examine these transitions in ML CWPS,

we calculate the kinetic switching pathways using the climbing image nudged elastic band method, a widely proven tool for modeling such transitions [71]. Our results [Fig. 3(g)] show that ML CWPS has an AFE ground state and a metastable FE state. The AFE-to-FE transition occurs when $E_\epsilon > E_{B1}$, while the FE-to-AFE transition is driven by a reversed ϵ with $E_\epsilon > E_{B2}$. To avoid switching the FE state to its opposite \mathbf{P} , the ϵ should satisfy $E_{B2} < E_\epsilon < E_{B1,3}$, where E_{B3} represents the energy barrier through the paraelectric (PE) state. The calculated E_{B1} (E_{B2} , E_{B3}) in ML CWPS is 0.33 (0.15, 0.37) eV/f.u., comparable with similar transitions in CuInP₂S₆ and CuCrP₂S₆, where a weak ϵ (tens of kV/cm) can experimentally drive the AFE-FE transition [65,72]. Given the structural and polarization similarities among these materials, we estimate that an ϵ of similar magnitude should be sufficient to induce phase transitions in the CWPS system. This highlights the potential of CWPS for ϵ control of \mathbf{P} and \mathbf{P}_S .

Expanding our focus to other multiferroics, we explore 3D oxide perovskites, highlighting the broad applicability of our design principle across various material dimensions and types. Traditional AFE perovskites, such as PbZrO₃, PbHfO₃, and NaNbO₃, have been studied for their applications in energy storage, sensors, and memory devices [46]. By including magnetic atoms, multiferroic perovskites, as exemplified with BiFeO₃, have been extensively

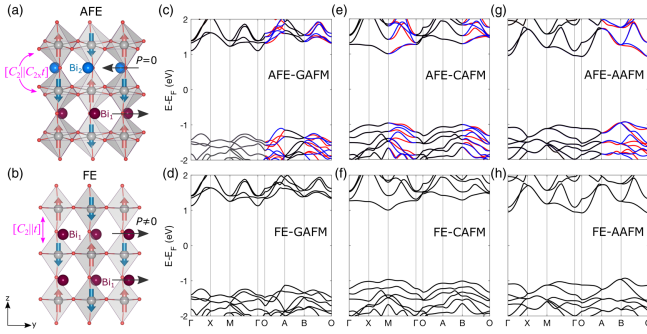


FIG. 4. (a) Structure of BiCrO_3 showing AFE-GAFM ground state with their spin lattices connected by $C_{2x}t$. (b) As in (a) but showing FE-GAFM state with spin lattices connected by t . (c), (d) Spin-resolved bands for (a)–(b), respectively. (e),(f) and (g), (h) As in (c),(d), but for CAFM, and AAFM states, respectively.

studied [73,74]. We consider a multiferroic BiCrO_3 to demonstrate our design principle due to its known coexistence of AFE and AFM properties [75,76]. In its ground state, as shown in Fig. 4(a), BiCrO_3 is a G-type AFM (GAFM) and belongs to the $Pbnm$ space group. Its AFE behavior results from the opposing displacements of the adjacent Bi atoms. ϵ can shift the Bi atoms to the same side [76], changing the system from AFE to FE states as in Fig. 4(b). Our calculations show that its ground state of AFE-GAFM gives AFEAM, characterized by the $[C_2||C_{2x}t]$, exhibiting altermagnetic spin splitting [Fig. 4(c)]. For FE-GAFM case, its spin lattices are directly connected by $[C_2||t]$, showing FEAFM [Fig. 4(d)]. Such phenomenon in BiCrO_3 further corroborates our design principle in Fig. 1.

While BiCrO_3 predominantly exhibits GAFM, we have also explored the common C-type (CAFM) and A-type (AAFM) orders of AFM in perovskites [55]. Similar to AFE-GAFM, both AFE-CAFM and AFE-AAFM BiCrO_3 display AM with spin splitting along distinct paths [Figs. 4(e) and 4(g)], but this splitting disappears in their FE phases [Figs. 4(f) and 4(h)]. Our findings on such altermagnetic behavior in BiCrO_3 can be directly extended to other similar perovskites by substituting its Bi or Cr elements [55,77,78], provided that the materials retain the AFE and AFM configurations. The abundance of such perovskites enriches the scope for further experimental validation of how altermagnetic spin splitting is affected by magnetic orders and crystalline directions.

Our research establishes a universal design principle for AFEAM, positioning them as integral components of multiferroic materials. This design provides a versatile platform to explore magnetoelectric coupling influenced by the interplay between ferroelectricity and magnetism. The ability to electrically control the transition between AFEAM ($\mathbf{P} = 0$, $\mathbf{P}_s \neq 0$) and FEAFM ($\mathbf{P} \neq 0$, $\mathbf{P}_s = 0$) with a small ϵ , not only opens new avenues for investigating electrically controlled spintronics but also enhances their potential in multiferroics, particularly in tunnel junctions [14]. While there is a debate about the

terminology and the origin of the concepts of AM and nonrelativistic spin splitting, studied for decades [15], our findings are not limited to that debate as they offer unexplored opportunities for magnetoelectric coupling and novel classes of multiferroics, independent of the specific terminological details and if the SOC will invalidate a strict AM definition. Notably, unlike spin torque to electrically control magnetism [2,3], our electric control does not require magnetization reversal and can be realized using a small ϵ , thereby enhancing both the speed and the energy efficiency of potential devices.

Moreover, just as the discovery of 2D FM have advanced opportunities for designing vdW heterostructures, with the prospect of a growing family of 2D AM, it would be important to understand how they can transform the neighboring materials through proximity effects [79–82]. Since electric control of topological properties is already considered in various heterostructures [9,83], we expect that our proposal for electrically controlled vdW multiferroics, with multiple broken symmetries, can further expand the family of topological states and facilitate their manipulation, not only in the normal [40,84], but also in superconducting states [36,85–87].

Note added—After the completion of our work, we were made aware of two relevant studies [88,89] on magnetoelectric coupling in altermagnets.

Acknowledgments—We acknowledge Cheng Zhang, Yuan Lu, and Cheng Song for valuable discussions about their related experimental efforts. Tong Zhou thanks Avery Zhou and Mila Zhou for their inspiration. This work is supported by the National Natural Science Foundation of China (Grants No. 12474155, No. 12447163, No. 12488101, and No. 11904250), the Zhejiang Provincial Natural Science Foundation of China (LR25A040001), the Innovation Program for Quantum Science and Technology (Grant No. 2021ZD0302800), and the Air Force Office of Scientific Research under Award No. FA9550-22-1-0349 (Y. L., I. Ž.). The computational resources for this research were provided by the High Performance Computing Platform at the Eastern Institute of Technology, Ningbo.

X. D. and J. Z. contributed equally to this work.

- [1] I. Žutić, J. Fabian, and S. Das Sarma, Spintronics: Fundamentals and applications, *Rev. Mod. Phys.* **76**, 323 (2004).
- [2] E. Y. Tsymbal and I. Žutić, eds., *Spintronics Handbook Spin Transport and Magnetism*, 2nd Edition (CRC Press, Taylor & Francis, Boca Raton, FL, 2019).
- [3] H. Yang, S. Valenzuela, M. Chshiev, S. Couet, B. Dieny, B. Drubak, A. Fert, K. Garello, M. Jamet, D. Jeong, K. Lee, T. Lee, M. Martin, G. Kar, P. Séneor, H. Shin, and S. Roche, Two-dimensional materials prospects for non-volatile spintronic memories, *Nature (London)* **606**, 663 (2022).

- [4] P. Dainone *et al.*, Controlling the helicity of light by electrical magnetization switching, *Nature (London)* **627**, 783 (2024).
- [5] W. Eerenstein, N. Mathur, and J. Scott, Multiferroic and magnetoelectric materials, *Nature (London)* **442**, 759 (2006).
- [6] M. Fiebig, T. Lottermoser, D. Meier, and M. Trassin, The evolution of multiferroics, *Nat. Rev. Mater.* **1**, 16046 (2016).
- [7] S. Dong, H. Xiang, and E. Dagotto, Magnetoelectricity in multiferroics: A theoretical perspective, *Natl. Sci. Rev.* **6**, 629 (2019).
- [8] H. S. Røsing, B. Fraser, S. M. Griffin, S. Bandyopadhyay, A. Mahabir, S.-W. Cheong, and A. V. Balatsky, Axion-matter coupling in multiferroics, *Phys. Rev. Res.* **3**, 033236 (2021).
- [9] J. Chen, P. Cui, and Z. Zhang, Ferroelectricity-tuned band topology and superconductivity in 2D materials and related heterostructures, *Adv. Funct. Mater.* **34**, 2408625 (2024).
- [10] N. Hill, Why are there so few magnetic ferroelectrics?, *J. Phys. Chem. B* **104**, 6694 (2000).
- [11] V. Baltz, A. Manchon, M. Tsoi, T. Moriyama, T. Ono, and Y. Tserkovnyak, Antiferromagnetic spintronics, *Rev. Mod. Phys.* **90**, 015005 (2018).
- [12] L. Šmejkal, Y. Mokrousov, B. Yan, and A. MacDonald, Topological antiferromagnetic spintronics, *Nat. Phys.* **14**, 242 (2018).
- [13] H. Chen, L. Liu, X. Zhou, Z. Meng, X. Wang, Z. Duan, G. Zhao, H. Yan, P. Qin, and Z. Liu, Emerging antiferromagnets for spintronics, *Adv. Mater.* **36**, 2310379 (2024).
- [14] D. Shao and E. Tsymbal, Antiferromagnetic tunnel junctions for spintronics, *npj Spintron.* **2**, 13 (2024).
- [15] S. Pekar and E. Rashba, Combined resonance in crystals in inhomogeneous magnetic fields, *Zh. Eksp. Teor. Fiz.* **47**, 1927 (1964) [*J. Exp. Theor. Phys.* **20**, 1295 (1965)].
- [16] D. Litvin and W. Opechowski, Spin groups, *Physica (Utrecht)* **76**, 538 (1974).
- [17] L.-D. Yuan, Z. Wang, J.-W. Luo, E. I. Rashba, and A. Zunger, Giant momentum-dependent spin splitting in centrosymmetric low-Z antiferromagnets, *Phys. Rev. B* **102**, 014422 (2020).
- [18] S. Hayami, Y. Yanagi, and H. Kusunose, Bottom-up design of spin-split and reshaped electronic band structures in antiferromagnets without spin-orbit coupling: Procedure on the basis of augmented multipoles, *Phys. Rev. B* **102**, 144441 (2020).
- [19] H. Ma, M. Hu, N. Li, J. Liu, W. Yao, J. Jia, and J. Liu, Multifunctional antiferromagnetic Materials with giant piezomagnetism and noncollinear spin current, *Nat. Commun.* **12**, 2846 (2021).
- [20] J. M. D. Coey, *Magnetism and Magnetic Materials*, 2nd Edition (Cambridge University Press, Cambridge, England, 2024).
- [21] L. Šmejkal, J. Sinova, and T. Jungwirth, Emerging research landscape of altermagnetism, *Phys. Rev. X* **12**, 040501 (2022).
- [22] I. Mazin, Altermagnetism then and now, *Physics* **17**, 4 (2024).
- [23] J. Krempaský, L. Šmejkal, S. D’Souza, M. Hajlaoui, G. Springholz, K. Uhlířová, F. Alarab, P. Constantinou, V. Strocov, D. Usanov, W. Pudelko, R. González-Hernández, A. Birk Hellenes, Z. Jansa, H. Reichlová, Z. Šobáň, R. Gonzalez Betancourt, P. Wadley, J. Sinova, D. Kriegner, J. Minár, J. Dil, and T. Jungwirth, Altermagnetic lifting of Kramers spin degeneracy, *Nature (London)* **626**, 517 (2024).
- [24] T. Osumi, S. Souma, T. Aoyama, K. Yamauchi, A. Honma, K. Nakayama, T. Takahashi, K. Ohgushi, and T. Sato, Observation of a giant band splitting in altermagnetic MnTe, *Phys. Rev. B* **109**, 115102 (2024).
- [25] S. Lee, S. Lee, S. Jung, J. Jung, D. Kim, Y. Lee, B. Seok, J. Kim, B. Park, L. Šmejkal, C.-J. Kang, and C. Kim, Broken Kramers degeneracy in altermagnetic MnTe, *Phys. Rev. Lett.* **132**, 036702 (2024).
- [26] S. Reimers, L. Odenbreit, L. Šmejkal, V. Strocov, P. Constantinou, A. Hellenes, R. Jaeschke Ubiergo, W. Campos, V. Bharadwaj, A. Chakraborty, T. Claudia, W. Shi, R. Dunin-Borkowski, S. Das, M. Klaui, J. Sinova, and M. Jourdan, Direct observation of altermagnetic band splitting in CrSb thin films, *Nat. Commun.* **15**, 2116 (2024).
- [27] J. Ding *et al.*, Large band-splitting in *g*-wave type altermagnet CrSb, *Phys. Rev. Lett.* **133**, 206401 (2024).
- [28] M. Zeng, M. Zhu, Y. Zhu, X. Liu, X. Ma, Y. Hao, P. Liu, G. Qu, Y. Yang, Z. Jiang, K. Yamagami, M. Arita, X. Zhang, T. Shao, Y. Dai, K. Shimada, Z. Liu, M. Ye, Y. Huang, Q. Liu, and C. Liu, Observation of spin splitting in room-temperature metallic antiferromagnet CrSb, *Adv. Sci.* **11**, 2406529 (2024).
- [29] G. Yang, Z. Li, S. Yang, J. Li, H. Zheng, W. Zhu, S. Cao, W. Zhao, J. Zhang, M. Ye, Y. Song, L.-H. Hu, L. Yang, M. Shi, H. Yuan, Y. Zhang, Y. Xu, and Y. Liu, Three-dimensional mapping and electronic origin of large altermagnetic splitting near Fermi level in CrSb, *arXiv:2405.12575*.
- [30] R. González-Hernández, L. Šmejkal, K. Výborný, Y. Yahagi, J. Sinova, T. Jungwirth, and J. Železný, Efficient electrical spin splitter based on nonrelativistic collinear antiferromagnetism, *Phys. Rev. Lett.* **126**, 127701 (2021).
- [31] L. Šmejkal, A. B. Hellenes, R. González-Hernández, J. Sinova, and T. Jungwirth, Giant and tunneling magnetoresistance in unconventional collinear antiferromagnets with nonrelativistic spin-momentum coupling, *Phys. Rev. X* **12**, 011028 (2022).
- [32] Q. Cui, Y. Zhu, X. Yao, P. Cui, and H. Yang, Giant spin-Hall and tunneling magnetoresistance effects based on a two-dimensional nonrelativistic antiferromagnetic metal, *Phys. Rev. B* **108**, 024410 (2023).
- [33] K. Samanta, Y.-Y. Jiang, T. R. Paudel, D.-F. Shao, and E. Y. Tsymbal, Tunneling magnetoresistance in magnetic tunnel junctions with a single ferromagnetic electrode, *Phys. Rev. B* **109**, 174407 (2024).
- [34] D. Zhu, Z.-Y. Zhuang, Z. Wu, and Z. Yan, Topological superconductivity in two-dimensional altermagnetic metals, *Phys. Rev. B* **108**, 184505 (2023).
- [35] B. Brekke, A. Brataas, and A. Sudbø, Two-dimensional altermagnets: Superconductivity in a minimal microscopic model, *Phys. Rev. B* **108**, 224421 (2023).
- [36] S. A. A. Ghorashi, T. L. Hughes, and J. Cano, Altermagnetic routes to Majorana modes in zero net magnetization, *Phys. Rev. Lett.* **133**, 106601 (2024).

- [37] T. P. T. Nguyen and K. Yamauchi, *Ab initio* prediction of anomalous Hall effect in antiferromagnetic CaCrO_3 , *Phys. Rev. B* **107**, 155126 (2023).
- [38] R. D. Gonzales Betancourt, J. Zubáč, R. Gonzalez-Hernandez, K. Geishendorf, Z. Šobáň, G. Springholz, K. Olejník, L. Šmejkal, J. Sinova, T. Jungwirth, S. T. B. Goennenwein, A. Thomas, H. Reichlová, J. Železný, and D. Kriegner, Spontaneous anomalous Hall effect arising from an unconventional compensated magnetic phase in a semiconductor, *Phys. Rev. Lett.* **130**, 036702 (2023).
- [39] Z. Zhou, X. Cheng, M. Hu, J. Liu, F. Pan, and C. Song, Manipulation of the altermagnetic order in CrSb via crystal symmetry, *Nature (London)* **638**, 645 (2025).
- [40] P. Guo, Z. Liu, and Z. Lu, Quantum anomalous Hall effect in collinear antiferromagnetism, *npj Comput. Mater.* **9**, 70 (2023).
- [41] D.-F. Shao, Y.-Y. Jiang, J. Ding, S.-H. Zhang, Z.-A. Wang, R.-C. Xiao, G. Gurung, W.J. Lu, Y.P. Sun, and E.Y. Tsymbal, Néel spin currents in antiferromagnets, *Phys. Rev. Lett.* **130**, 216702 (2023).
- [42] R.-W. Zhang, C. Cui, R. Li, J. Duan, L. Li, Z.-M. Yu, and Y. Yao, Predictable gate-field control of spin in altermagnets with spin-layer coupling, *Phys. Rev. Lett.* **133**, 056401 (2024).
- [43] K. S. Denisov and I. Žutić, Anisotropic spin dynamics in antiferromagnets with a nonrelativistic spin splitting, *Phys. Rev. B* **110**, L180403 (2024).
- [44] Z. Jin, Z. Zeng, Y. Cao, and P. Yan, Skyrmion Hall effect in altermagnets, *Phys. Rev. Lett.* **133**, 196701 (2024).
- [45] M. Susner, M. Chyasanavichyus, M. McGuire, P. Ganesh, and P. Maksymovych, Metal thio- and selenophosphates as multifunctional van der Waals layered materials, *Adv. Mater.* **29**, 1602852 (2017).
- [46] Y. Si, T. Zhang, C. Liu, S. Das, B. Xu, R. Burkovsky, X. Wei, and Z. Chen, Antiferroelectric oxide thin-films: Fundamentals, properties, and applications, *Prog. Mater. Sci.* **142**, 101231 (2024).
- [47] Y. Noda, K. Ohno, and S. Nakamura, Momentum-dependent band spin splitting in semiconducting MnO_2 : A density functional calculation, *Phys. Chem. Chem. Phys.* **18**, 13294 (2016).
- [48] T. Okugawa, K. Ohno, Y. Noda, and S. Nakamura, Weakly spin-dependent band structures of antiferromagnetic perovskite LaMO_3 ($M = \text{Cr}, \text{Mn}, \text{Fe}$), *J. Phys. Condens. Matter* **30**, 075502 (2018).
- [49] Y. Jiang, Z. Song, T. Zhu, Z. Fang, H. Weng, Z.-X. Liu, J. Yang, and C. Fang, Enumeration of spin-space groups: Toward a complete description of symmetries of magnetic orders, *Phys. Rev. X* **14**, 031039 (2024).
- [50] Z. Xiao, J. Zhao, Y. Li, R. Shindou, and Z.-D. Song, Spin space groups: Full classification and applications, *Phys. Rev. X* **14**, 031037 (2024).
- [51] X. Chen, J. Ren, Y. Zhu, Y. Yu, A. Zhang, P. Liu, J. Li, Y. Liu, C. Li, and Q. Liu, Enumeration and representation theory of spin space groups, *Phys. Rev. X* **14**, 031038 (2024).
- [52] P. Liu, J. Li, J. Han, X. Wan, and Q. Liu, Spin-group symmetry in magnetic materials with negligible spin-orbit coupling, *Phys. Rev. X* **12**, 021016 (2022).
- [53] X. Chen, Y. Liu, P. Liu, Y. Yu, J. Ren, J. Li, A. Zhang, and Q. Liu, Catalog of unconventional magnons in collinear magnets, [arXiv:2307.12366](https://arxiv.org/abs/2307.12366).
- [54] F. Xue, Y. Ma, H. Wang, L. Luo, Y. Xu, T. D. Anthopoulos, M. Lanza, B. Yu, and X. Zhang, Two-dimensional ferroelectricity and antiferroelectricity for next-generation computing paradigms, *Matter Radiat. Extremes* **5**, 1999 (2022).
- [55] See Supplemental Material at <http://link.aps.org/supplemental/10.1103/PhysRevLett.134.106801>, which includes Refs. [56–61], for the expanded discussion of the effective model, first-principles calculation methods, and the influence of transition metals, magnetic configurations, spin-orbit coupling, layer thickness, and Hubbard U values.
- [56] P. E. Blöchl, Projector augmented-wave method, *Phys. Rev. B* **50**, 17953 (1994).
- [57] G. Kresse and J. Furthmüller, Efficient iterative schemes for *ab initio* total-energy calculations using a plane-wave basis set, *Phys. Rev. B* **54**, 11169 (1996).
- [58] J. P. Perdew, K. Burke, and M. Ernzerhof, Generalized gradient approximation made simple, *Phys. Rev. Lett.* **77**, 3865 (1996).
- [59] S. L. Dudarev, G. A. Botton, S. Y. Savrasov, C. J. Humphreys, and A. P. Sutton, Electron-energy-loss spectra and the structural stability of nickel oxide: An LSDA + U study, *Phys. Rev. B* **57**, 1505 (1998).
- [60] G. Henkelman, B. P. Uberuaga, and H. Jónsson, A climbing image nudged elastic band method for finding saddle points and minimum energy paths, *J. Chem. Phys.* **113**, 9901 (2000).
- [61] C. Himcinschi, I. Vrejoiu, T. Weißbach, K. Vijayanandhini, A. Talkenberger, C. Röder, S. Bahmann, D. R. T. Zahn, A. A. Belik, D. Rafaja, and J. Kortus, Raman spectra and dielectric function of BiCrO_3 : Experimental and first-principles studies, *J. Appl. Phys.* **110**, 073501 (2011).
- [62] J. Qi, H. Wang, X. Chen, and X. Qian, Two-dimensional multiferroic semiconductors with coexisting ferroelectricity and ferromagnetism, *Appl. Phys. Lett.* **113**, 043102 (2018).
- [63] C. Hua, H. Bai, Y. Zheng, Z. Xu, S. A. Yang, Y. Lu, and S. Wei, Strong coupled magnetic and electric ordering in monolayer of metal thio(seleno)phosphates, *Chin. Phys. Lett.* **38**, 077501 (2021).
- [64] W. Io, S. Pang, L. Wong, Y. Zhao, R. Ding, J. Mao, Y. Zhao, F. Guo, S. Yuan, J. Zhao, J. Yi, and J. Hao, Direct observation of intrinsic room-temperature ferroelectricity in 2D layered CuCrP_2S_6 , *Nat. Commun.* **14**, 7304 (2023).
- [65] X. Wang, Z. Shang, C. Zhang, J. Kang, T. Liu, X. Wang, S. Chen, H. Liu, W. Tang, Y. Zeng, J. Guo, Z. Cheng, L. Liu, D. Pan, S. Tong, B. Wu, Y. Xie, G. Wang, J. Deng, T. Zhai, H. Deng, J. Hong, and J. Zhao, Electrical and magnetic anisotropies in van der Waals multiferroic CuCrP_2S_6 , *Nat. Commun.* **14**, 840 (2023).
- [66] Q. Hu, Y. Huang, Y. Wang, S. Ding, M. Zhang, C. Hua, L. Li, X. Xu, J. Yang, S. Yuan, K. Watanabe, T. Taniguchi, Y. Lu, C. Jin, D. Wang, and Y. Zheng, Ferrielectricity controlled widely-tunable magnetoelectric coupling in van der Waals multiferroics, *Nat. Commun.* **15**, 3029 (2024).
- [67] D. Yu, Y. Ga, J. Liang, C. Jia, and H. Yang, Voltage-controlled Dzyaloshinskii-Moriya interaction torque switching of perpendicular magnetization, *Phys. Rev. Lett.* **130**, 056701 (2023).

- [68] X. Duan, H. Wang, X. Chen, and J. Qi, Multiple polarization phases and strong magnetoelectric coupling in the layered transition metal phosphorus chalcogenides TMP_2X_6 ($\text{T} = \text{Cu}, \text{Ag}$; $\text{M} = \text{Cr}, \text{V}$; $\text{X} = \text{S}, \text{Se}$) by controlling the interlayer interaction and dimension, *Phys. Rev. B* **106**, 115403 (2022).
- [69] C. Huang, J. Feng, F. Wu, D. Ahmed, B. Huang, H. Xiang, K. Deng, and E. Kan, Toward intrinsic room-temperature ferromagnetism in two-dimensional semiconductors, *J. Am. Chem. Soc.* **140**, 11519 (2018).
- [70] Y. Zhu *et al.*, Observation of plaid-like spin splitting in a noncoplanar antiferromagnet, *Nature (London)* **626**, 523 (2024).
- [71] Z. Guan, Y. Zhao, X. Wang, N. Zhong, X. Deng, Y. Zheng, J. Wang, D. Xu, R. Ma, F. Yue, Y. Cheng, R. Huang, P. Xiang, Z. Wei, J. Chu, and C. Duan, Electric-field-induced room-temperature antiferroelectric–ferroelectric phase transition in van der Waals layered GeSe, *ACS Nano* **16**, 1308 (2022).
- [72] S. M. Neumayer, Z. Zhao, A. O’Hara, M. A. McGuire, M. A. Susner, S. T. Pantelides, P. Maksymovych, and N. Balke, Nanoscale control of polar surface phases in layered van der Waals CuInP_2S_6 , *ACS Nano* **16**, 2452 (2022).
- [73] J. Yang, Q. He, P. Yu, and Y. Chu, BiFeO_3 Thin films: A playground for exploring electric-field control of multifunctionalities, *Annu. Rev. Mater. Res.* **45**, 249 (2015).
- [74] M. U. Farooq, Z. Gui, and L. Huang, Spontaneous spin momentum locking and anomalous Hall effect in BiFeO_3 , *Phys. Rev. B* **107**, 075202 (2023).
- [75] N. Hill, P. Bättig, and C. Daul, First principles search for multiferroism in BiCrO_3 , *J. Phys. Chem. B* **106**, 3383 (2002).
- [76] D. Kim, H. Lee, M. Varela, and H. Christen, Antiferroelectricity in multiferroic BiCrO_3 epitaxial films, *Appl. Phys. Lett.* **89**, 162904 (2006).
- [77] L. Ding, P. Manuel, D. D. Khalyavin, F. Orlandi, Y. Kumagai, F. Oba, W. Yi, and A. A. Belik, Unusual magnetic structure of the high-pressure synthesized perovskites ACrO_3 ($\text{A} = \text{Sc}, \text{In}, \text{Tl}$), *Phys. Rev. B* **95**, 054432 (2017).
- [78] J. A. McLeod, Z. V. Pchelkina, L. D. Finkelstein, E. Z. Kurmaev, R. G. Wilks, A. Moewes, I. V. Solovyev, A. A. Belik, and E. Takayama-Muromachi, Electronic structure of BiMO_3 multiferroics and related oxides, *Phys. Rev. B* **81**, 144103 (2010).
- [79] I. Žutić, A. Matos-Abiague, B. Scharf, H. Dery, and K. Belashchenko, Proximity-induced materials, *Mater. Today* **22**, 85 (2019).
- [80] F. Ibrahim, A. Hallal, D. Lerma, X. Waintal, E. Tsymbal, and M. Chshiev, Unveiling multiferroic proximity effect in graphene, *2D Mater.* **7**, 015020 (2020).
- [81] W. Sun, H. Ye, L. Liang, N. Ding, S. Dong, and S.-S. Wang, Stacking-dependent ferroicity of a reversed bilayer: Alternating magnetism or ferroelectricity, *Phys. Rev. B* **110**, 224418 (2024).
- [82] S.-D. Guo, Y. Liu, J. Yu, and C.-C. Liu, Valley polarization in twisted altermagnets, *Phys. Rev. B* **110**, L220402 (2024).
- [83] T. Zhou, S. Cheng, M. Schleienvoigt, P. Schüffelen, H. Jiang, Z. Yang, and I. Žutić, Quantum spin-valley Hall Kink states: From concept to materials design, *Phys. Rev. Lett.* **127**, 116402 (2021).
- [84] R. M. Fernandes, V. S. de Carvalho, T. Birol, and R. G. Pereira, Topological transition from nodal to nodeless Zeeman splitting in altermagnets, *Phys. Rev. B* **109**, 024404 (2024).
- [85] Y.-X. Li and C.-C. Liu, Majorana corner modes and tunable patterns in an altermagnet heterostructure, *Phys. Rev. B* **108**, 205410 (2023).
- [86] T. Zhou, M. C. Dartailh, K. Sardashti, J. E. Han, A. Matos-Abiague, J. Shabani, and I. Žutić, Fusion of Majorana bound states with mini-gate control in two-dimensional systems, *Nat. Commun.* **13**, 1738 (2022).
- [87] M. Amundsen, J. Linder, J. W. A. Robinson, I. Žutić, and N. Banerjee, Colloquium: Spin-orbit effects in superconducting hybrid structures, *Rev. Mod. Phys.* **96**, 021003 (2024).
- [88] M. Gu, Y. Liu, H. Zhu, K. Yananose, X. Chen, Y. Hu, A. Stroppa, and Q. Liu, following Letter, Ferroelectric switchable altermagnetism, *Phys. Rev. Lett.* **134**, 106802 (2025).
- [89] L. Šmejkal, Altermagnetic multiferroics and altermagnetoelectric effect, [arXiv:2411.19928](https://arxiv.org/abs/2411.19928).

Supplemental Material

Antiferroelectric Altermagnets: Antiferroelectricity Alters Magnets

Xunkai Duan^{1,2}, Jiayong Zhang^{1,3,4}, Ziye Zhu^{1,4}, Yuntian Liu⁵,

Zhenyu Zhang⁴, Igor Žutić⁵, and Tong Zhou^{1,*}

¹Eastern Institute for Advanced Study, Eastern Institute of Technology, Ningbo, Zhejiang 315200, China

²School of Physics and Astronomy, Shanghai Jiao Tong University, Shanghai 200240, China

³School of Physical Science and Technology, Suzhou University of Science and Technology, Suzhou 215009, China

⁴International Center for Quantum Design of Functional Materials (ICQD), and Hefei National Laboratory, University of Science and Technology of China, Hefei, 230026, China

⁵Department of Physics, University at Buffalo, State University of New York, Buffalo, NY 14260, USA

Corresponding author email: *tzhou@eitech.edu.cn

I. Effective Model

II. First-Principles Calculation Methods

III. Electronic Structures of CuMP₂S(Se)₆ (*M* = Cr, Mo, W) and the Influence of *M*

IV. Influence of Magnetic Configurations in CuWP₂S₆

V. Influence of Layer Thickness in CuWP₂S₆

VI. Structures and Magnetic Configurations of BiCrO₃-like Perovskites

VII. Influence of the Spin-Orbit Coupling

I. Effective Model

To further illustrate our design principle for antiferroelectric altermagnets (AFEAM) in Fig. 1, we develop an effective tight-binding (TB) model based on a general 2D rectangular lattice with nested antiferromagnetic order (Fig. S1). This setup includes the essential elements of our proposal: antiferromagnet (AFM) sublattices with ferroelectric (FE) and antiferroelectric (AFE) configurations connected by t and C_2t symmetries, respectively. The minimal model, capturing the influence of AFE and FE states on altermagnetism, is required to incorporate up to the third-nearest-neighbor interactions

$$H = \left(\sum_{i,j} \left(f_i^{\eta_j} c_i^\dagger c_{i+\eta_j} + g_i^{\kappa_j} c_i^\dagger c_{i+\kappa_j} + h_i^{\delta_j} c_i^\dagger c_{i+\delta_j} \right) + h.c. \right) + M_{A,B} \sum_{i \in A,B} c_i^\dagger \sigma_z c_i.$$

Here, $c_i^\dagger (c_i)$ are electron creation (annihilation) operators at site i and σ is the Pauli matrix. The first three terms describe hopping between first (NN), second (2NN), and third (3NN) nearest-neighbors with hopping parameters $f_i^{\eta_j}$, $g_i^{\kappa_j}$, and $h_i^{\delta_j}$, where η_j , κ_j , and δ_j are the vectors connecting site i to its NN, 2NN, 3NN sites. The last term indicates AFM exchange fields on sublattices A and B with $M_A = -M_B$.

Our symmetry analysis in main text demonstrates the emergence of AM arises from the inequivalence between magnetic sublattices. However, as shown in Fig. S1, NN and 2NN hoppings are sublattice-equivalent under both AFE and FE configurations ($f_A^{\eta_{1-6}} = f_B^{\eta_{1-6}}$ and $g_A^{\kappa_{1-6}} = g_B^{\kappa_{1-6}}$), thus not contributing to AM. In contrast, 3NN hoppings, occurring only within the same sublattice, are dependent on the sublattice and (A)FE configurations, playing a crucial role in AM. For FEAFM, $[C_2||t]$ symmetry ensures that 3NN hopping parameters between opposite sublattices are equivalent ($h_A^{\delta_{1-6}} = h_B^{\delta_{1-6}}$) [Fig. S1(f)]. Consequently, the calculated bands exhibit spin degeneracy, characteristic of conventional AFM [Fig. 2(d)]. Conversely, the AFE configuration breaks t symmetry, leaving magnetic sublattices connected by $[C_2||C_2t]$ symmetry. This symmetry alters the 3NN hopping parameters such that hopping along $\delta_{1,4}$ in sublattice A ($h_A^{\delta_{1,4}}$) differs from that in sublattice B ($h_B^{\delta_{1,4}}$) but equals the hopping along $\delta_{2,5}$ ($h_B^{\delta_{2,5}}$) in sublattice B, and vice versa, i.e. $h_A^{\delta_{1,4}} = h_B^{\delta_{2,5}} \neq h_B^{\delta_{1,4}} = h_A^{\delta_{2,5}} \neq h_A^{\delta_{3,6}} = h_B^{\delta_{3,6}}$ as depicted in Fig. S1(c). This directional alternation induces altermagnetic spin splitting, as confirmed by the calculated band structures in Fig. 2(c).

Based on the preceding discussions, we conclude that our developed effective TB model accurately demonstrate the mechanism of our design principle for AFEAM and reveal how the AFE configurations create the hopping inequivalence between sublattices and induce the altermagnetism. Such a model provides a new tool to understand and design the AFEAM and to explore possible device applications.

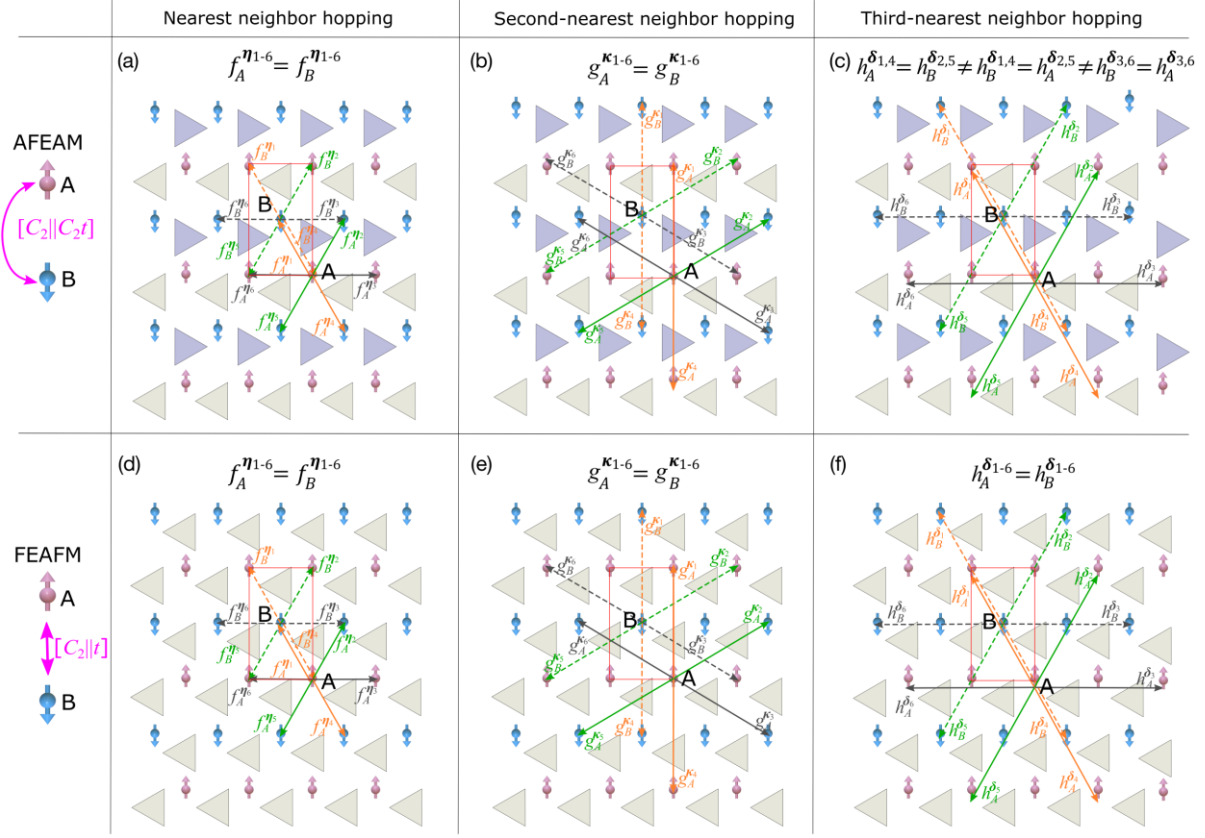


Fig. S1. Schematic of 2D rectangular magnetic sublattices A and B with AFE (distinct triangles) and FE (identical triangles) configurations, forming AFEAM with $[C_2||C_2t]$ symmetry and FEAFM with $[C_2||t]$ symmetry, respectively. (a)-(c) and (d)-(f) illustrate NN, 2NN, and 3NN hoppings for AFEAM and FEAFM, where the solid (dashed) arrows indicate NN (η_{1-6}), 2NN (κ_{1-6}), and 3NN (δ_{1-6}) vectors from site A (B) with corresponding hopping strengths $f_{A,B}^{\eta_{1-6}}$, $g_{A,B}^{\kappa_{1-6}}$, and $h_{A,B}^{\delta_{1-6}}$, respectively. NN and 2NN hoppings are sublattice-equivalent under both AFE and FE configurations ($f_A^{\eta_{1-6}} = f_B^{\eta_{1-6}}$ and $g_A^{\kappa_{1-6}} = g_B^{\kappa_{1-6}}$), thus not contributing to AM. In contrast, 3NN hoppings are dependent on sublattices and (A)FE configurations, playing a crucial role in AM. For AFEAM, they are sublattice-inequivalent ($h_A^{\delta_{1,4}} = h_B^{\delta_{2,5}} \neq h_B^{\delta_{1,4}} = h_A^{\delta_{2,5}} \neq h_A^{\delta_{3,6}} = h_B^{\delta_{3,6}}$) due to $[C_2||C_2t]$ symmetry, leading to AM. Conversely, for FEAFM, they are sublattice-equivalent ($h_A^{\delta_{1-6}} = h_B^{\delta_{1-6}}$) due to the $[C_2||t]$ symmetry, giving conventional AFM.

II. First-Principles Calculation Methods

The geometry optimization and electronic structure calculations of the studied material systems are performed with the projector augmented-wave (PAW) [1] formalism by using the first-principles calculations method based on density functional theory (DFT), as implemented in the Vienna *ab initio* simulation package (VASP) [2]. The Perdew-Burke-Ernzerhof generalized gradient approximation (GGA-PBE) is employed to describe the exchange and correlation functional [3]. The energy cutoff of the plane-wave and the convergence criteria of the total energy are set to be 600 eV and 10^{-6} eV, respectively. All atoms in the unit cell are allowed to relax until the Hellmann-Feynman force on each atom is smaller than 0.001 eV/Å. All parameters have been checked to ensure the results are converged. For two-dimensional (2D) films, a vacuum space larger than 20 Å is used to avoid the interaction between the neighboring slabs. To take into account the correction effects of d electrons, the GGA+ U method [4] is adopted. For CuMP₂S(Se)₆ (M = Cr, Mo, W) system, the values of the effective Hubbard U_{eff} are set to be 3.0, 1.0 and 1.0 eV for Cr, Mo, and W atoms, respectively, which have been proven to accurately describe their electronic structures [5]. For BiCrO₃, we use $U_{\text{eff}}=3$ eV for Cr atoms, consistent with values widely reported to describe the electronic structure of BiCrO₃ [6]. The climbing image nudged elastic band (CI-NEB) method is used to obtain the kinetic switching pathways [7].

To further assess the impact of U_{eff} , we performed U_{eff} -dependent calculations for monolayer (ML) CuWP₂S₆ and BiCrO₃. The results (Table S1) show that the magnetic ground states are independent on U_{eff} . While the band gap increases with U_{eff} , as commonly observed, the band splitting of interest is minimally affected (Fig. S2), demonstrating the robustness of our conclusions against variations in U_{eff} .

Table S1. U_{eff} -dependent total energy of various magnetic configurations for AFE and FE ML CuWP₂S₆ and BiCrO₃. The total energy of the ground state is taken as the reference value (0), in units of meV/formula units (f.u.). The red indicates the chosen U_{eff} in our work.

Material	U_{eff} (eV)	sAFM	zAFM	FM
CuWP ₂ S ₆	$U_{\text{eff}}=1$	0	5.28	45.15
		183.90	189.46	255.08
	$U_{\text{eff}}=2$	0	4.29	29.37
		194.69	199.20	220.47
	$U_{\text{eff}}=3$	0	3.55	18.48
		205.08	208.76	220.20
		GAFM	CAFM	AAFM
BiCrO ₃	$U_{\text{eff}}=2$	0	29.26	92.42
		774.00	826.22	863.40
	$U_{\text{eff}}=3$	0	26.69	79.66
		790.35	835.32	868.48
	$U_{\text{eff}}=4$	0	25.03	70.66
		806.60	847.63	877.55
				97.04
				933.82

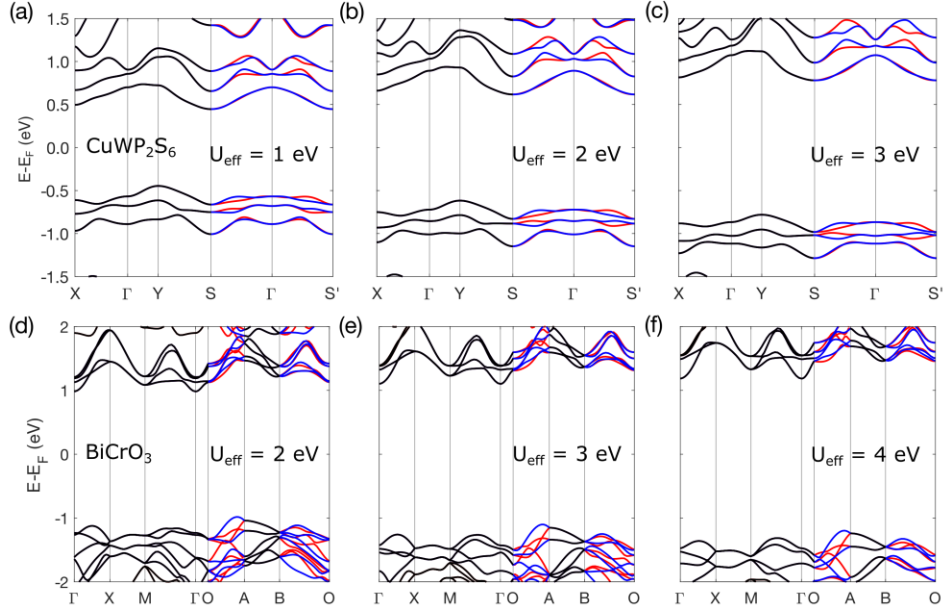


Fig. S2. U_{eff} -dependent bands for the ground state of ML CuWP₂S₆ (AFE-sAFM) and BiCrO₃ (AFE-GAFM).

III. Electronic Structures of CuMP₂S(Se)₆ ($M = \text{Cr, Mo, W}$) and the Influence of M

We have systematically explored the electronic structure and magnetic properties of the CuWP₂S₆ (CWPS) in the main text. Similar to CWPS, the CuWP₂S(Se)₆, CuCrP₂S(Se)₆ and CuMoP₂S(Se)₆ also show AFEAM when they are in the sAFM state as indicated in Fig. S3. However, their magnetic ground state depends on the M atom. Specifically, our calculations (Table S2) indicate the ML CuCrP₂S(Se)₆ favors FM, while MLs of CuMoP₂S(Se)₆ and CuWP₂S(Se)₆ favor sAFM, consistent with the previous studies and experiments [5,8-11]. As a result, the ground CuCrP₂S(Se)₆ is not our desired AFEAM, although it has been well-explored in experiments. This M -type dependency is attributed to the combined effect of the crystal field splitting and superexchange interaction induced by M based on the superexchange theorem [5,12,13].

In CuMP₂S(Se)₆ compounds, due to the $MS(\text{Se})_6$ octahedral crystal field, the $M-d$ orbitals split into two parts: the lower-energy threefold degenerate orbitals, t_{2g} , and higher-energy twofold degenerate orbitals, e_g . The t_{2g} is partially filled, while the e_g remains empty, making these systems magnetic semiconductors. According to the superexchange theory, for an intrinsic magnetic semiconducting system, increasing (decreasing) the virtual exchange gap, G_{ex} , between the occupied and empty orbitals can effectively enhance the antiferromagnetism (ferromagnetism) [12,13]. Since the G_{ex} in CuMP₂S(Se)₆ increases as the M orbital radius increases [5], the G_{ex} in CuCrP₂S(Se)₆ is smaller than that in CuMoP₂S(Se)₆ and CuWP₂S(Se)₆. Despite the complex lattice structure and multiple exchange paths, the small G_{ex} in CuCrP₂S(Se)₆ makes it favor ferromagnetism, while the large G_{ex} in CuMoP₂S(Se)₆ and CuWP₂S(Se)₆ makes them favor antiferromagnetism, as confirmed by our calculations.

Table S2. The total energy of various magnetic states for AFE and FE configurations in ML CuMP₂S(Se)₆ ($M = \text{Cr, Mo, W}$). The total energy of ground state for each material is taken as the reference value (0), in units of meV/f.u.

Material	Configuration	sAFM	zAFM	FM
CuWP ₂ Se ₆	AFE	0	6.35	68.45
	FE	142.68	151.25	200.64
CuWP ₂ S ₆	AFE	0	5.28	45.15
	FE	183.90	189.46	255.08
CuMoP ₂ Se ₆	AFE	0	4.94	14.44
	FE	145.92	149.83	150.85
CuMoP ₂ S ₆	AFE	0	1.90	3.48
	FE	175.48	178.00	172.56
CuCrP ₂ Se ₆	AFE	21.33	29.53	0
	FE	207.74	215.39	176.68
CuCrP ₂ S ₆	AFE	19.68	30.50	0
	FE	189.92	197.72	160.08

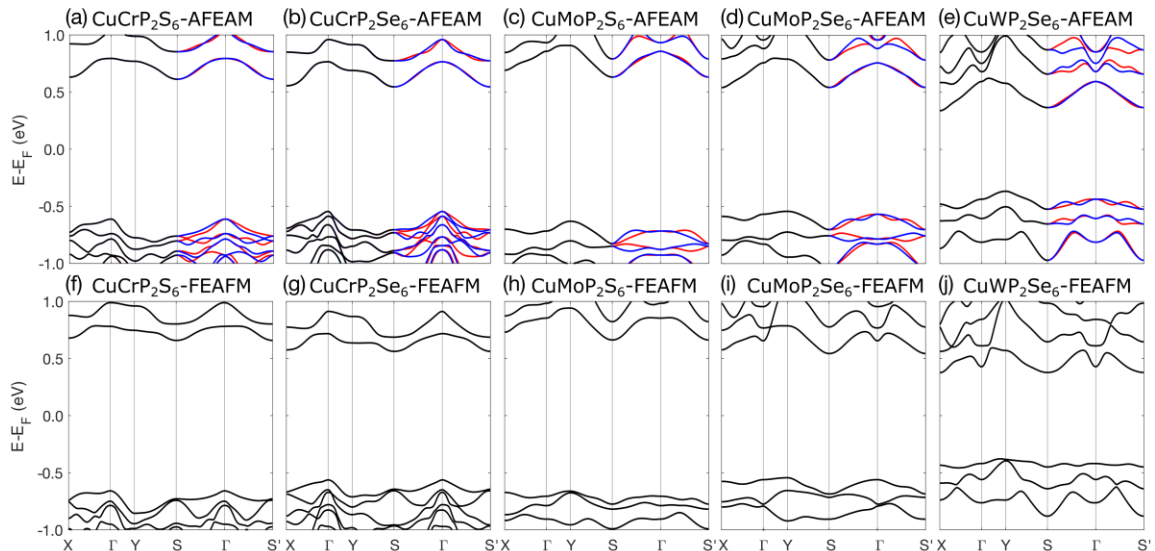


Fig. S3 (a)-(e) the same as Fig. 3(c) but for AFE-sAFM CuCrP₂S₆, CuCrP₂Se₆, CuMoP₂S₆, CuMoP₂Se₆, and CuWP₂Se₆, respectively. (f)-(j) the same as Fig. 3(d) but for FE-sAFM CuCrP₂S₆, CuCrP₂Se₆, CuMoP₂S₆, CuMoP₂Se₆, and CuWP₂Se₆, respectively.

IV. Influence of Magnetic Configurations in CuWP₂S₆

To understand the relevance of magnetic configuration to AM, we explored zAFM configuration, which is energetically less favorable by ~ 5 meV/f.u., compared to the ground state sAFM in ML CWPS (Table S2). Unlike AFE-sAFM, the spin lattices in (A)FE-zAFM can be directly connected by $[C_2||t]$, showing conventional AFM properties, as shown in Fig. S4. The results [Fig. S4(a) and S4(b)] of sAFM ML CWPS are recalculated using 2×1 supercells to match the unit cell of its zAFM for a better comparison.

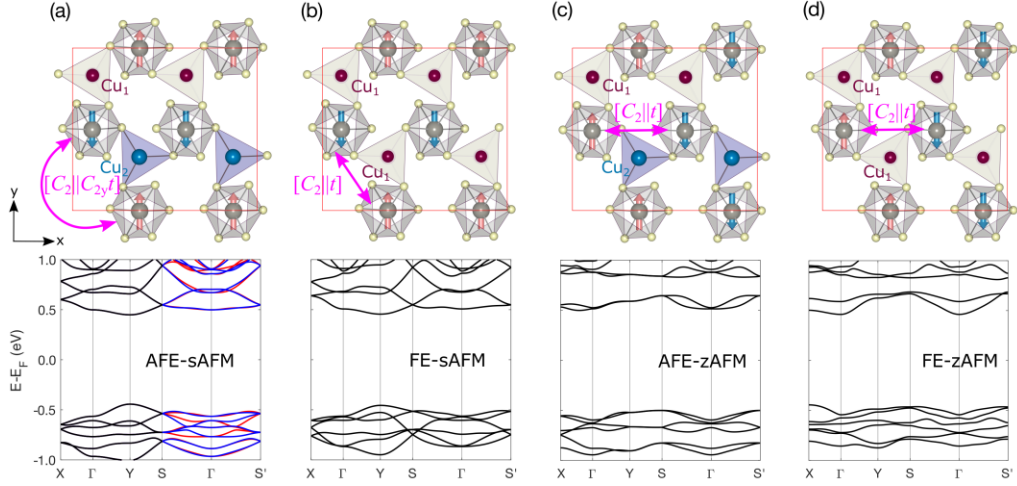


Fig. S4 (a) and (b) Same as Figs. 3(a) and 3(b) but for supercells (2×1) of sAFM ML CWPS. (c) and (d) Same as (a) and (b) but for zAFM ML CWPS.

V. Influence of Layer Thickness in CuWP₂S₆

The electronic structures and magnetic properties of ML and bulk CWPS have been extensively demonstrated in the main text, revealing the behavior of AM and AFM in its AFE and FE states, respectively. Given that CWPS is a vdW material, it is anticipated that its few-layer films would exhibit properties similar to those of its ML and bulk forms. To explore this, we conducted calculations for bilayer and trilayer CWPS films, as depicted in Fig. S5. Our results indicate that the AFE CWPS films are AM, while its FE states are AFM. These findings confirm that the magnetic orders and electronic structures of the bilayer and trilayer films are consistent with those observed in their ML and bulk counterparts. This agreement across different thicknesses reinforces the feasibility of the experimental realization of our proposal.

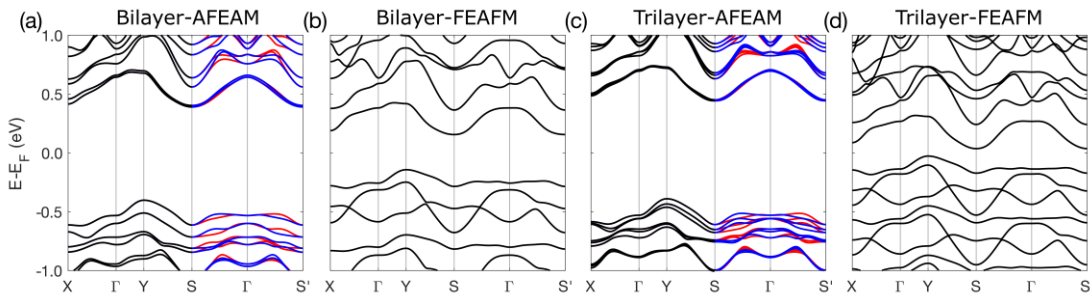


Fig. S5 (a)-(b) and (c)-(d) Same as Figs. 2(c)-2(d) but for bilayer and trilayer CuWP₂S₆, respectively.

VI. Structures and Magnetic Configurations of BiCrO₃-like Perovskites

For BiCrO₃, its ground state is AFE-GAFM as shown in Table S3, and transitioning to the FE state does not alter its magnetic state, consistent with prior research [14,15]. The side views of the AFE and FE BiCrO₃ structures, along with their G-type AFM configurations, are presented in Fig. 4 of the main text. In Figs. S6(a) and S6(b), we provide the top views of these structures, where the AFE and FE orders are distinctly visible through the different (or identical) displacements of the Bi₁ and Bi₂ atoms. Figures S6(c)-S6(h) illustrate the schematics of the G-type, C-type, and A-type AFM for both AFE and FE BiCrO₃. Additionally, Fig. S6(i) shows the specific paths used for the band structure calculations presented in Fig. 4.

As discussed in the main text, BiCrO₃ is identified as an AFEAM candidate from both symmetry analysis and band calculations. This symmetry-driven principle enables us to expand these findings to other similar perovskites by substituting its nonmagnetic (Bi) and magnetic (Cr) elements. For instance, the Bi atoms can be replaced by elements such as Sc, In, and Tl [16], while the Cr atoms can be substituted with Co, Mn, Fe, and Ni [17]. According to our design principle and symmetry description, as long as these materials are in the AFE-AFM state, they exhibit spin-polarized AFEAM behavior, while they show spin-degenerate FEAFM behavior in the FE-AFM state.

Table S3. Same as Table S2, but for BiCrO₃ in units of meV/f.u.

		GAFM	CAFM	AAFM	FM
BiCrO ₃	AFE	0	26.69	79.66	109.78
	FE	790.35	835.32	868.48	933.13

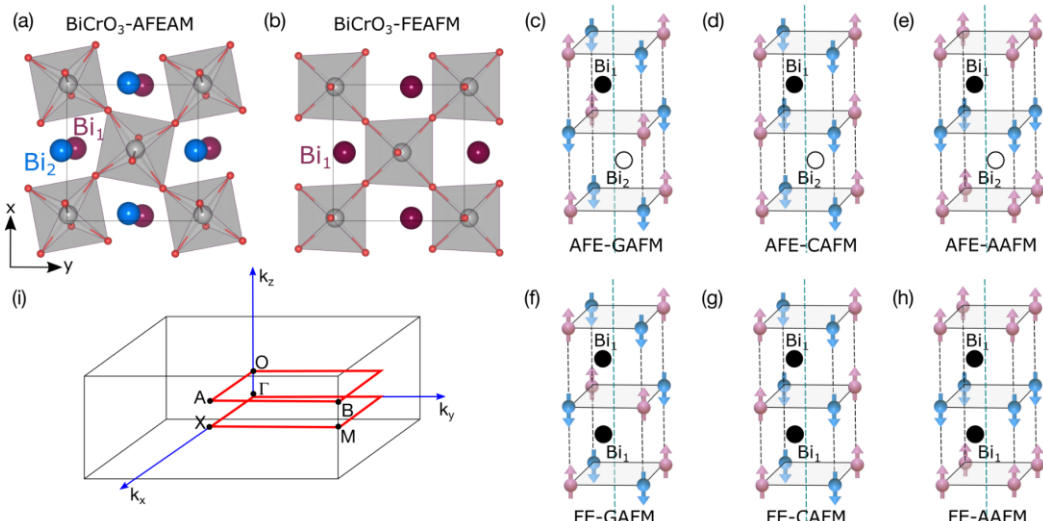


Fig. S6. (a) and (b) Side view of Figs. 4(a) and 4(b), respectively. (c)-(e) Schematic of G-type, C-type, and A-type AFM for AFE BiCrO₃. (f)-(h) Same as (c)-(d) but for FE BiCrO₃. The red and blue arrows indicate the positive and negative magnetic moments, respectively. The black (Bi₁) and white (Bi₂) circles indicate the different displacements of Bi atoms. (i) The Brillouin zone of BiCrO₃, with specific paths (red) for bands in Fig. 4, where the coordinates of Γ , X, M, O, A, and B are (0, 0, 0), (0.5, 0, 0), (0.5, 0.5, 0), (0, 0, 0.25), (0.5, 0, 0.25), and (0.5, 0.5, 0.25), respectively.

VII. Influence of the Spin-Orbit Coupling

The spin splitting in altermagnets is a nonrelativistic effect that generally excludes considerations of spin-orbit coupling (SOC). Nevertheless, SOC is invariably present in real materials, making it crucial to investigate its impact on the spin polarization in our proposed AFEAM and FEAFM systems. Typically, the AFEAM (with spin polarization) and FEAFM (with spin degeneracy) hinge on the breaking and preserving of time-reversal symmetry, respectively. Given that SOC does not alter time-reversal symmetry, the electric control of spin polarization in AFEAM remains unaffected by SOC. Notably, AFEAM can exhibit classic ferromagnetic behavior, such as spin-polarized currents and anomalous Hall effects [18-20]—phenomena absent in FEAFM. Thus, AFEAM and FEAFM can be clearly distinguished using these spin-related measurements, regardless of the presence of SOC.

Experimentally, altermagnetism is often identified using angle-resolved photoemission spectroscopy (ARPES), previously employed for MnTe [21], and CrSb [22]. This method depends on the distinguishability of the altermagnetic spin splitting. If the SOC-induced spin splitting significantly exceeds altermagnetic spin splitting, it could obscure the identification of altermagnetism. To address this, we have calculated the band structure with SOC for our proposed AFEAM candidates, CuWP₂S₆ and BiCrO₃. The SOC-induced spin splitting in these materials is smaller than the altermagnetic spin splitting as in Fig. S7. This substantial difference is expected to be detectable through ARPES. Furthermore, the SOC-induced spin splitting typically necessitates heavy atoms; however, our design principle is universally applicable to the (A)FE order, independent of specific elemental requirements. By focusing on the light-element AFEAM, we can further suppress the SOC effects, thus enhancing the feasibility of experimentally observing our proposed mechanisms in real materials, even with the consideration of SOC. Furthermore, since, unlike the SOC, AM break the time-reversal symmetry and can display typical ferromagnetic properties, we can use spin transport to distinguish altermagnetic and SOC spin splitting [23,24].

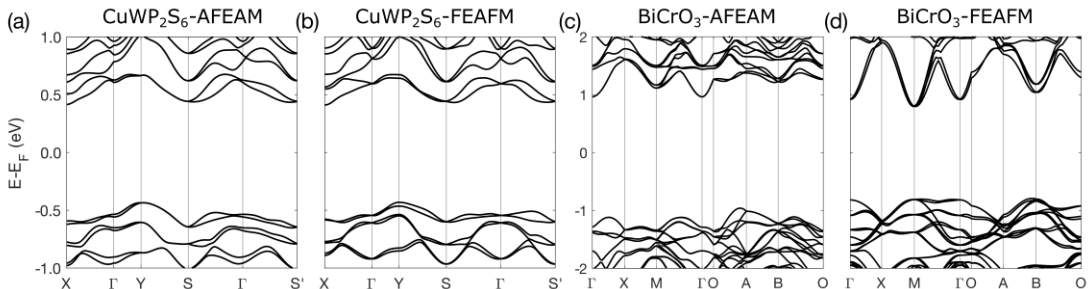


Fig. S7 (a)-(b) and (c)-(d) Same as Figs. 2(c)-2(d) and Figs. 4(c)-4(d) but with SOC, respectively.

References

- [1] P. E. Blochl, Projector Augmented-Wave Method, *Phys. Rev. B* **50**, 17953 (1994).
- [2] G. Kresse and J. Furthmuller, Efficient iterative schemes for ab initio total-energy calculations using a plane-wave basis set, *Phys. Rev. B* **54**, 11169 (1996).
- [3] J. P. Perdew, K. Burke, and M. Ernzerhof, Generalized gradient approximation made simple, *Phys. Rev. Lett.* **77**, 3865 (1996).
- [4] S. L. Dudarev, G. A. Botton, S. Y. Savrasov, C. J. Humphreys, and A. P. Sutton, Electron-energy-loss spectra and the structural stability of nickel oxide: An LSDA+U study, *Phys. Rev. B* **57**, 1505 (1998).
- [5] C. Q. Hua, H. Bai, Y. Zheng, Z. A. Xu, S. Y. A. Yang, Y. H. Lu, and S. H. Wei, Strong Coupled Magnetic and Electric Ordering in Monolayer of Metal Thio(seleno)phosphates, *Chin. Phys. Lett.* **38**, 077501 (2021).
- [6] C. Himcinschi, I. Vrejoiu, T. Weißbach, K. Vijayanandhini, A. Talkenberger, C. Röder, S. Bahmann, Di. R. T. Zahn, A. A. Belik, D. Rafaja and J. Kortus, Raman spectra and dielectric function of BiCrO₃: Experimental and first-principles studies, *J. Appl. Phys.* **110**, 073501 (2011).
- [7] G. Henkelman, B. P. Uberuaga, and H. Jónsson, A climbing image nudged elastic band method for finding saddle points and minimum energy paths, *J. Chem. Phys.* **113**, 9901 (2000).
- [8] J. S. Qi, H. Wang, X. F. Chen, and X. F. Qian, Two-dimensional multiferroic semiconductors with coexisting ferroelectricity and ferromagnetism, *Appl. Phys. Lett.* **113**, 043102 (2018).
- [9] W. F. Io, S. Y. Pang, L. W. Wong, Y. Q. Zhao, R. Ding, J. F. Mao, Y. F. Zhao, F. Guo, S. G. Yuan, J. Zhao, J. B. Yi, and J. H. Hao, Direct observation of intrinsic room-temperature ferroelectricity in 2D layered CuCrP₂S₆, *Nat. Commun.* **14**, 7304 (2023).
- [10] X. L. Wang, Z. X. Shang, C. Zhang, J. Q. Kang, T. Liu, X. Y. Wang, S. L. Chen, H. L. Liu, W. Tang, Y. J. Zeng, J. F. Guo, Z. H. Cheng, L. Liu, D. Pan, S. C. Tong, B. Wu, Y. Y. Xie, G. C. Wang, J. X. Deng, T. R. Zhai, H. X. Deng, J. W. Hong, and J. H. Zhao, Electrical and magnetic anisotropies in van der Waals multiferroic CuCrP₂S₆, *Nat. Commun.* **14**, 840 (2023).
- [11] Q. F. Hu, Y. Q. Huang, Y. Wang, S. J. Ding, M. J. Zhang, C. Q. Hua, L. J. Li, X. F. Xu, J. B. Yang, S. J. Yuan, K. Watanabe, T. Taniguchi, Y. H. Lu, C. H. Jin, D. W. Wang, and Y. Zheng, Ferrielectricity controlled widely-tunable magnetoelectric coupling in van der Waals multiferroics, *Nat. Commun.* **15**, 3029 (2024).
- [12] X. K. Duan, H. Wang, X. F. Chen, and J. S. Qi, Multiple polarization phases and strong magnetoelectric coupling in the layered transition metal phosphorus chalcogenides TMP₂X₆ (T = Cu, Ag; M = Cr, V; X = S, Se) by controlling the interlayer interaction and dimension, *Phys. Rev. B* **106**, 115403 (2022).
- [13] C. X. Huang, J. S. Feng, F. Wu, D. Ahmed, B. Huang, H. J. Xiang, K. M. Deng, and E. J. Kan, Toward Intrinsic Room-Temperature Ferromagnetism in Two-Dimensional Semiconductors, *J. Am. Chem. Soc.* **140**, 11519 (2018).

- [14] N. A. Hill, P. Bättig, and C. Daul, First principles search for multiferroism in BiCrO_3 , *J. Phys. Chem. B* **106**, 3383 (2002).
- [15] D. H. Kim, H. N. Lee, M. Varela, and H. M. Christen, Antiferroelectricity in multiferroic BiCrO_3 epitaxial films, *Appl. Phys. Lett.* **89**, 162904 (2006).
- [16] L. Ding, P. Manuel, D. D. Khalyavin, F. Orlandi, Y. Kumagai, F. Oba, W. Yi, and A. A. Belik, Unusual magnetic structure of the high-pressure synthesized perovskites $ACrO_3$ ($A = \text{Sc}, \text{In}, \text{Tl}$), *Phys. Rev. B* **95**, 054432 (2017).
- [17] J. A. McLeod, Z. V. Pchelkina, L. D. Finkelstein, E. Z. Kurmaev, R. G. Wilks, A. Moewes, I. V. Solovyev, A. A. Belik, and E. Takayama-Muromachi, Electronic structure of BiMO_3 multiferroics and related oxides, *Phys. Rev. B* **81**, 144103 (2010).
- [18] R. González-Hernández, L. Šmejkal, K. Výborný, Y. Yahagi, J. Sinova, T. Jungwirth, and J. Železný, Efficient Electrical Spin Splitter Based on Nonrelativistic Collinear Antiferromagnetism, *Phys. Rev. Lett.* **126**, 127701 (2021).
- [19] R. Gonzalez Betancourt, J. Zubáč, R. Gonzalez-Hernandez, K. Geishendorf, Z. Šobáň, G. Springholz, K. Olejník, L. Šmejkal, J. Sinova, and T. Jungwirth, Spontaneous anomalous Hall effect arising from an unconventional compensated magnetic phase in a semiconductor, *Phys. Rev. Lett.* **130**, 036702 (2023).
- [20] P. J. Guo, Z. X. Liu, and Z. Y. Lu, Quantum anomalous Hall effect in collinear antiferromagnetism, *npj Comput. Mater.* **9**, 70 (2023).
- [21] J. Krempasky, L. Smejkal, S. W. D'Souza, M. Hajlaoui, G. Springholz, K. Uhlírová, F. Alarab, P. C. Constantinou, V. Strocov, D. Usanov, W. R. Pudelko, R. González-Hernández, A. B. Hellenes, Z. Jansa, H. Reichlová, Z. Sobán, R. D. G. Betancourt, P. Wadley, J. Sinova, D. Kriegner, J. Minár, J. H. Dil, and T. Jungwirth, Altermagnetic lifting of Kramers spin degeneracy, *Nature* **626**, 517 (2024).
- [22] S. Reimers, L. Odenbreit, L. Smejkal, V. N. Strocov, P. Constantinou, A. B. Hellenes, R. J. Ubiergo, W. H. Campos, V. K. Bharadwaj, A. Chakraborty, T. Denneulin, W. Shi, R. E. Dunin-Borkowski, S. Das, M. Kläui, J. Sinova, and M. Jourdan, Direct observation of altermagnetic band splitting in CrSb thin films, *Nat. Commun.* **15**, 2116 (2024).
- [23] D. F. Shao and E. Y. Tsymbal, Antiferromagnetic tunnel junctions for spintronics, *npj Spintron.* **2**, 13 (2024).
- [24] K. Samanta, Y. Y. Jiang, T. R. Paudel, D. F. Shao, and E. Y. Tsymbal, Tunneling magnetoresistance in magnetic tunnel junctions with a single ferromagnetic electrode, *Phys. Rev. B* **109**, 174407 (2024).